







Closing the hybridization charge gap in the Kondo semiconductor SmB_6 with an ultrahigh magnetic field

Daisuke Nakamura ^{1,2,*} Atsushi Miyake ¹ Akihiko Ikeda ^{1,3} Masashi Tokunaga ¹
Fumitoshi Iga ⁴ and Yasuhiro H. Matsuda ^{1,†}

¹*The Institute for Solid State Physics, The University of Tokyo, Kashiwa, Chiba 277-8581, Japan*

²*RIKEN Center for Emergent Matter Science (CEMS), Hirosawa, Wako, Saitama 351-0198, Japan*

³*Department of Engineering Science, University of Electro-Communications, Chofu, Tokyo 182-8585, Japan*

⁴*Institute of Quantum Beam Science, Ibaraki University, Mito, Ibaraki 310-8512, Japan*



(Received 9 August 2021; revised 10 May 2022; accepted 16 May 2022; published 6 June 2022)

We have investigated the high-frequency magnetoresistance of Kondo semiconductor SmB_6 under ultrahigh magnetic fields generated by the electromagnetic flux-compression technique. The semiconductor-metal transition due to closing of the hybridization charge gap was observed at approximately 180 T. The critical magnetic field observed is substantially higher than that reported previously. At temperatures below around 10 K, another transition was observed at a lower field (approximately 80 T). We suggest that the observed 80-T transition relates with the energy scale of quasiparticles such as the spin polaron in the in-gap state.

DOI: [10.1103/PhysRevB.105.L241105](https://doi.org/10.1103/PhysRevB.105.L241105)

I. INTRODUCTION

In materials with strong electron correlation, the nontrivial energy-band structure beyond the single-electron picture gives rise to exotic properties. For example, itinerant and localized electrons close to the Fermi level hybridize at low temperatures (Kondo hybridization), forming a nonmagnetic Kondo singlet. At the same time, a narrow energy gap can open through electron correlation, causing a metal to semiconductor transition in certain f electron based materials that have been termed Kondo semiconductors [1,2] such as SmB_6 , YbB_{12} , and $\text{Ce}_3\text{Bi}_4\text{Pt}$.

SmB_6 is a typical Kondo semiconductor, with a cubic CsCl-type crystal structure [3]. Its hybridization gap has been estimated to be 5–20 meV [4–7]. This relatively large range reflects a difficulty of evaluating the energy gap because of the complex electronic band structure around the hybridization gap [8]. Two f -electron states (Γ_7 and Γ_8) hybridize with that of the conduction electron in the vicinity of the Fermi level, inducing two hybridization gaps [9] (see also Supplemental Material [10] for the schematic band structure; also see Refs. [8,11–19]). In addition, the valence of the Sm ion fluctuates between $3+$ ($4f^5$, magnetic) and $2+$ ($4f^6$, nonmagnetic), giving an intermediate valence state of $\sim 2.6+$ (at 300 K) or $\sim 2.5+$ (at 5 K) [20,21]. Furthermore, a termination atom sensitive topological surface state [6,22] hinders the extraction of the bulk electronic band structure by surface-sensitive techniques such as angle-resolved photoemission measurements or scanning-tunneling microscopy.

Investigating the magnetoresistance in high magnetic fields can help to understand the complicated electronic states. Applied magnetic fields shift the energy bands by the Zeeman

effect; eventually, a field-induced semiconductor to metal (S-M) transition takes place, closing the hybridization gap. Considering the hybridization gap of SmB_6 (5–20 meV), an ultrahigh magnetic field exceeding 100 T is probably necessary for the energy gap to close, because the Zeeman energy of a free electron at 100 T is 12 meV. A magnetic field induced S-M transition has been predicted to occur at 107–125 T, extrapolating the measured low-field magnetoresistance up to 33 T [11,12]. Another study reported an unusual successive semiconductor-metal-semiconductor transition at 4 K [13]: Four-terminal DC resistivity measurement in a field of up to 145 T showed that the magnetoresistance continuously decreased up to 86 T, and then quadratically increased with further increase in the magnetic field. Such a “reentrant” semiconducting state seems to contradict the picture of Zeeman shift induced gap closure. In addition, such a reentrant semiconducting phase was not observed with the pressure-induced S-M transition [14]. Thus, the details of the magnetic field induced S-M transition in SmB_6 remain unclear.

II. EXPERIMENT

In the present work, a single crystal of SmB_6 was grown by the floating-zone method using an image furnace with four xenon lamps [23]. The DC electrical resistivity ρ_{DC} in the absence of a magnetic field was measured with 10 Hz AC bias mode of Physical Properties Measurement System (PPMS). The standard four-terminal AC electrical resistivity with a 50-kHz bias voltage was measured under high magnetic fields up to 55 T, which were generated by a nondestructive (ND) pulsed magnet (pulse duration of 35 ms). The magnetic field was applied parallel to the $\langle 100 \rangle$ axis of the SmB_6 crystal and perpendicular to the current path [$\langle 100 \rangle // B \perp I$].

Higher magnetic fields up to 320 T with the duration time of several microseconds were generated by the electromagnetic flux-compression (EMFC) technique [15]. A

*daisuke.nakamura.rg@riken.jp

†ymatsuda@issp.u-tokyo.ac.jp

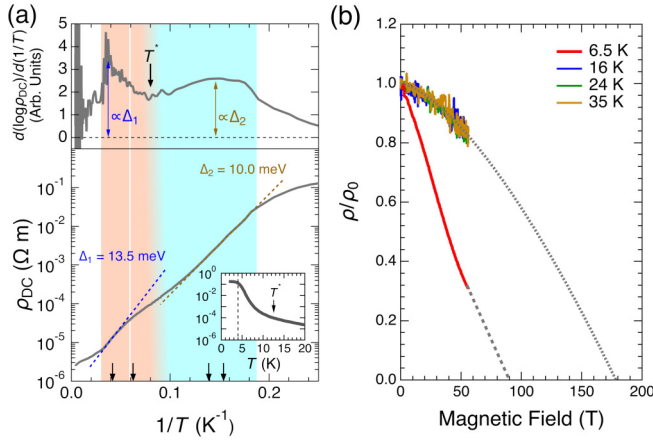


FIG. 1. Transport properties of SmB_6 samples. (a) Temperature (T) dependence of the DC electrical resistivity ρ_{DC} (bottom panel) and of $d(\log \rho_{DC})/d(1/T)$ (upper panel). The dotted guidelines are used for the evaluation of two energy scales, Δ_1 and Δ_2 . Arrows indicate reciprocals of measurement temperatures in high-field experiments. The characteristic temperature $T^* = 12.5$ K corresponds to the local minimum of $d(\log \rho_{DC})/d(1/T)$. The inset shows an enlarged view at low temperatures. (b) Normalized AC magnetoresistance ρ/ρ_0 measured up to 55 T at different temperatures, with extrapolations to higher field intensities.

small-scale “compact-EMFC” instrument with a maximum energy of 2 MJ was used in this work. The high-frequency electrical resistivity was measured using a recently developed contactless radio-frequency (rf) impedance-measurement method, the “self-resonant spiral coil” technique [16]. The measurement sample was mounted on a self-resonant spiral probe coil so that the $\langle 100 \rangle$ axis was parallel to the magnetic

field axis [see the inset of Fig. 2(a)]. An rf voltage tuned around 700 MHz was applied to the probe coil. The return rf signal was converted to electrical resistivity. Details of signal processing are described in the Supplemental Material [10] and Ref. [16]. The sample temperature T_{ini} was measured just before the magnetic field generation using a calibrated RuO_2 resistive thermometer.

III. RESULTS

The temperature dependence of ρ_{DC} in the absence of a magnetic field is shown in the bottom panel of Fig. 1(a). The residual resistivity ratio [RRR $\equiv \rho_{DC}(1.8 \text{ K})/\rho_{DC}(300 \text{ K})$] was 92 500, which is comparable to that of other high-quality SmB_6 crystals grown by the floating-zone method [24] and significantly larger than that of samples grown by the Al-flux method [12,13,25]. At ~ 4 K, ρ_{DC} saturated as shown in the inset, owing to topological surface conduction. In a previous work [26], a significant resistivity difference among samples of different thicknesses was observed only at temperatures lower than ~ 6 K. In addition, according to local/nonlocal transport measurement [27], most of the bias current ($\sim 90\%$) flows in the bulk state at 6 K. Thus, it can be said that the resistivity starts to be affected by the surface state only below ~ 6 K. To reveal the bulk nature, we performed the magnetoresistance measurements above 6.5 K in this work.

In Fig. 1(b), the AC magnetoresistance measured using a ND pulsed magnet is presented. Under magnetic fields up to 55 T and temperatures below 35 K, the magnetoresistance was negative, similar to previous high-field studies [11,12]. Here, ρ_0 is defined as the electrical resistivity under zero magnetic field. $\rho(B)/\rho_0$ between 16 and 35 K nearly overlapped, approaching zero near 180 T when we use $\rho(B) \propto -B^{3/2}$

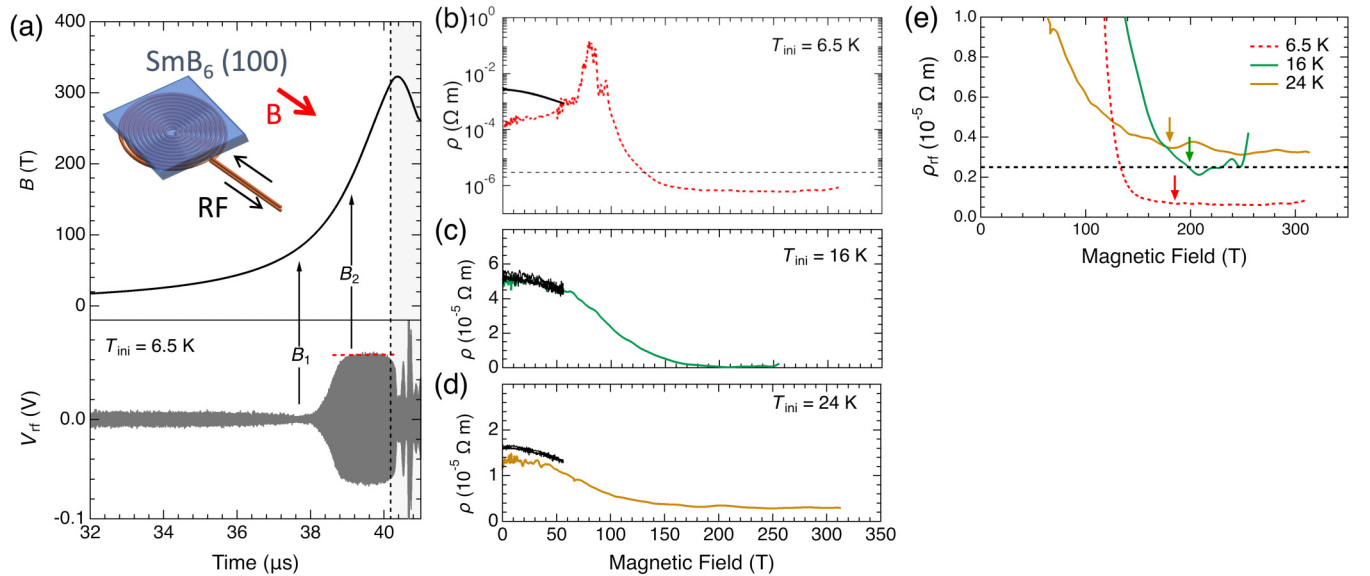


FIG. 2. Results of contactless radio-frequency (rf) impedance measurements up to 320 T. (a) Time evolution of (top) magnetic field B and (bottom) rf probe signal V_{rf} at the initial temperature 6.5 K. The inset is a schematic view of the measurement probe. (b)–(d) Magnetic-field dependence of the rf electrical resistivity (red, green, and brown curves) at (b) 6.5, (c) 16, and (d) 24 K. The AC magnetoresistances with 50 kHz up to 55 T are also presented for comparison (black curves). (e) Enlarged view of (b)–(d) around the field-induced metallic state. The semiconductor to metal transition fields are indicated by arrows, which correspond to B_2 shown in (a). The horizontal dashed line indicates the DC resistivity at 300 K in the absence of the field from Fig. 1(a).

as an extrapolation curve similar to Refs. [11,12]. On the other hand, $\rho(B)/\rho_0$ at 6.5 K decreases more rapidly. A tiny kink was observed around 45 T, and we used a linear function to extrapolate $\rho(B > 45 \text{ T})$; it approached -100% at approximately 90 T. Although this is a rough estimation of the transition field, the previous high-field studies reported a transition field close to ours [13,25].

The results of the EMFC experiments (at temperatures above 6 K, where the electrical resistivity was dominated by the bulk electronic state) are shown in Fig. 2. Around the peak magnetic field, an extrinsic-noise spike appeared in the high-frequency probe voltage V_{rf} ; it arose from destructive deformation of the EMFC magnet close to the measurement probe. In Fig. 2(a), V_{rf} gradually decreases and reaches a minimum (at $B_1 \sim 80 \text{ T}$). After that, it increases again and saturates at $B_2 \sim 180 \text{ T}$. $V_{\text{rf}}(t)$ values measured under different conditions are shown in the Supplemental Material [10].

The magnetic-field dependence of the rf resistivity converted from V_{rf} , $\rho_{\text{rf}}(B)$, at different temperatures is presented in Figs. 2(b)–2(d). The magnetoresistance up to 55 T from Fig. 1(b) is also presented for comparison. The values of $\rho_{\text{rf}}(B)$ at 16 and 24 K are in good agreement with the AC magnetoresistance up to 55 T, and continuously decrease up to $\sim 180 \text{ T}$. However, $\rho_{\text{rf}}(B)$ at 6.5 K is qualitatively different [Fig. 2(b)]: it increases with the field up to B_1 , and then gradually decreases. The saturation field (B_2) at 6.5 K seems to be comparable to those at higher temperatures, that is, $B_2 \sim 180 \text{ T}$. The peak in ρ_{rf} at $B_1 \sim 80 \text{ T}$ is reproducible, which is confirmed by an independent experiment at 7.2 K (see Supplemental Material [10] for the additional data at 7.2 K).

IV. DISCUSSION

First, sample characteristics are compared with those of flux-grown samples, because the different crystal growth methods of SmB_6 might cause different electronic excitations depending on the quality of crystal. In SmB_6 , a crystal grown by the floating-zone method used in this work, tends to introduce Sm vacancies [28], whereas that grown by the Al-flux method is contaminated by impurities from remnant flux [29]. However, possibly due to the refinement of the crystal growth technique, our sample shows similar characteristics to that of crystal grown by the Al-flux method. For the magnetic property, we confirmed that the magnitude of the Curie tail in the magnetic susceptibility below 20 K was quantitatively in good agreement with that in flux-grown crystals [17] (see Supplemental Material [10] for the magnetic susceptibility data). For the transport property, a resistance plateau below 4 K has not clearly appeared in the previous report using a floating-zone sample [30]. In contrast, our samples exhibit a clear resistance plateau below 4 K as shown in the inset of Fig. 1(a), similar to flux-grown crystals. Therefore, it is not unreasonable to conclude that intrinsic phenomena in SmB_6 are observed in the present study.

There seem to be two distinct temperature regions defined by differing electronic transport properties of SmB_6 , corresponding to the two broad hump structures [Fig. 1(a), top] in the temperature dependence of $d(\log \rho_{\text{DC}})/d(1/T)$; their boundary is at $T^* = 12.5 \text{ K}$. From the bottom panel of

Fig. 1(a), it is clear that $\log \rho_{\text{DC}}$ increases linearly with $(1/T)$ in a large portion of each regime (17–33 K and 5.5–9.0 K), but with different slopes. Accordingly, there are two energy scales ($\Delta_1 = 13.5 \text{ meV}$ and $\Delta_2 = 10 \text{ meV}$), assuming a thermal activation type conduction process, $\rho \propto \exp(-\Delta/2k_{\text{B}}T)$. Two different energy scales in $\rho(T)$ have also been reported previously [12]. For a different magnitude of $\rho(B)/\rho_0$ across T^* shown in Fig. 1(b), similar behavior is also reported in other high-field experiments using flux-grown samples [11,12] (also see Supplemental Material [10] for the comparison of $\rho(T)/\rho_0$ with different B values). These indicate that the existence of two distinct states across T^* is an intrinsic phenomenon in SmB_6 independent of the crystal growth method.

As shown in Fig. 2(e), the rf resistivity approaches the value in the temperature-induced metallic state (at $T = 300 \text{ K}$ and $B = 0 \text{ T}$, the horizontal dotted line) around $B_2 \sim 180 \text{ T}$. Therefore, we consider B_2 to be the S-M transition field where the hybridization charge gap closes. Hence, we term B_2 as B_{hyb} hereafter. As shown in Fig. 2(e), B_{hyb} exhibits no strong temperature dependence (also see Supplemental Material [10] for the data at 7.2 K). The continuous decrease in $\rho_{\text{rf}}(B)$ up to B_{hyb} at 16 and 24 K indicates a gradual suppression of the hybridization gap by the Zeeman-shift energy $E_z = \mu_{\text{eff}}B$, where the magnetic moment $\mu_{\text{eff}} = g_J m_J \mu_{\text{B}}$ (g_J is the Landé g factor; m_J is the magnetic quantum number of the total angular momentum J ; μ_{B} is the Bohr magneton). It was experimentally observed in YbB_{12} [31] that the Zeeman shift of the local moment of f electrons effectively explains the hybridization gap closure proportional to B . The Kondo hybridization in SmB_6 takes place between the d and Γ_7 or Γ_8 orbitals, resulting in two hybridization gaps [9] [$\Delta(\Gamma_7) > \Delta(\Gamma_8)$] (See Supplemental Material [10] for the schematic band structure). When $g_J m_J = 0.665$ for the Γ_8 state [32] and $B_{\text{hyb}} = 180 \text{ T}$ are used, $\Delta(\Gamma_8)$ is evaluated to be $2m_{\text{eff}}B_{\text{hyb}} = 13.9 \text{ meV}$, which is close to the previous evaluation (5–20 meV [4–7]).

However, the S-M transition field has been evaluated to be 85–90 T at 4 K in previous high-field studies [13,25]. This value is close to $B_1 \sim 80 \text{ T}$ in Fig. 2(b). Therefore, it is likely that the transition field reported in previous works corresponds to B_1 in the present work. We suppose that an anomalous transport property showing B_1 takes place only at temperatures below the characteristic temperature T^* . As shown in Figs. 2(b)–2(d), a notable difference between ρ_{rf} and the AC magnetoresistance is observed only at 6.5 K, in agreement with there being a boundary around $T^* \sim 12.5 \text{ K}$.

Here, we would like to discuss the dynamical character of the electrical resistivity and impedance of SmB_6 . The frequencies of the rf impedance measurement ($\sim 700 \text{ MHz}$), AC magnetoresistance measurement using the ND magnet (50 kHz), and previous high-field studies (DC [13], 274.5 kHz [25]) differ substantially. In the absence of a magnetic field, the frequency dependence of the resistivity in SmB_6 has already been investigated [18]. Interestingly, a notable decrease in high-frequency resistivity was observed below 10 K ($\sim T^*$). The temperature variations of the electrical resistivity at different frequencies are illustrated in Fig. 3(a), based on Refs. [4,18].

It is worth considering how low-temperature resistivity behaves as a function of frequency. According to Ref. [18], the Debye relaxation type spectrum $\rho_{\text{D}}(\omega = 2\pi f)$

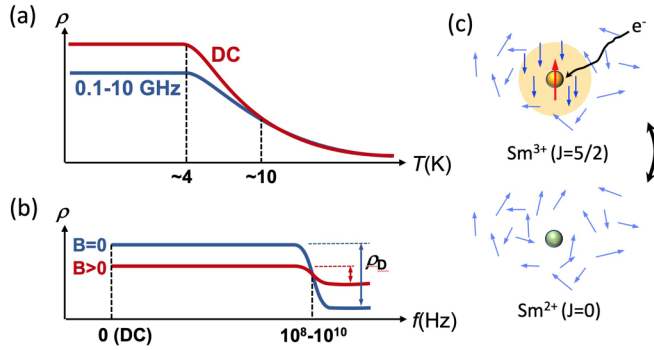


FIG. 3. Electronic conduction in SmB_6 . (a) $\rho(T)$ with different frequencies based on Refs. [4, 18]. (b) Assumed magnetic field evolution of $\rho(f)$ below critical temperature T^* . The curve for $B = 0$ is depicted based on Ref. [18]. (c) The spin polaron coupled with the valence fluctuation.

$\propto [\omega^2\tau/(1 + \omega^2\tau^2)]^{-1}$, with a typical frequency scale of 100 MHz–10 GHz, appears at low temperatures. The measurement frequency of the rf impedance measurement in the present work (700 MHz) is in the range where the Debye relaxation mechanism is significant and electron-hopping conduction is expected [18].

Using a Debye relaxation type spectrum, we assume the magnetic-field evolution of $\rho(f)$ shown in Fig. 3(b) (when $T < T^*$). If the amplitude of shoulderlike $\rho_D(f)$ is suppressed by increasing the magnetic field and 700 MHz is a high enough frequency to give a positive magnetoresistance, the steep increase in ρ_{rf} to B_1 can be explained.

Inelastic neutron-scattering experiments [33] imply the existence of a spin-related quasiparticle, the energy scale of which is smaller than the hybridization gap. The antiferromagnetic spin-polaronic state has been plausibly suggested as the spin-related quasiparticle for SmB_6 [18, 34–39]. If the Sm^{3+} ion ($J = 5/2$) couples with the surrounding spins antiferromagnetically, a spin-polaronic state can be formed [Fig. 3(c)]. This state can be dynamically fluctuated in SmB_6 because of the valence fluctuation of the Sm ion. When the Sm^{3+} ion ($J = 5/2$) changes to the Sm^{2+} ion ($J = 0$), annihilation of the spin polaron occurs with electron hopping, by which the amplitude of the Debye-type electrical-resistivity spectrum $\rho_D(f)$ is enhanced. Here, it is worth noting that the Sm valence-fluctuation timescale should be related to the typical frequency of $\rho_D(f)$ ($\tau^{-1} = 10^8$ – 10^{10} Hz, Ref. [18]). Although an early theoretical study [40] estimated a much faster valence fluctuation (on the order of 10^{-13} s), the comparison between the results of x-ray absorption and Mössbauer spectroscopy [20] suggests the slower timescale of an order of 10^{-8} s, which is comparable to τ in $\rho_D(f)$. The magnitude of $\rho_D(f)$ can be suppressed by the dissolution of the spin polaron into the free electron under sufficiently high magnetic fields. Therefore, the suppression of a spin-singlet spin polaron in the in-gap state can be one of the possible origins of the transition found at B_1 .

The temperature–magnetic field (T - B) phase diagram is constructed based on the experimental findings in the present study as shown in Fig. 4. The temperature evolution in the sample during the EMFC experiments is evaluated (thin

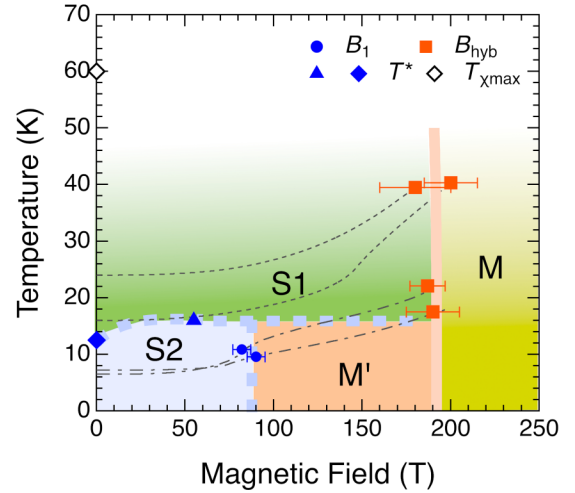


FIG. 4. Temperature–magnetic field phase diagram. S1: semiconductor dominating interband transition across the hybridization gap; S2: semiconductor dominating in-gap quasiparticle excitation; M': metallic region without closing the hybridization gap; M: field-induced metal after closing the hybridization gap. B_1 (closed circle) and B_{hyb} (closed square) are taken from the results of the electromagnetic flux-compression experiments; critical temperature T^* (closed triangle and diamond) is taken from the nondestructive experiment and Fig. 1(a). Each state is separated by bold guidelines for a clear view. The thin dashed-dotted and dotted curves indicate the temperature evolution during the magnetic-field pulse.

dashed-dotted and dotted curves in Fig. 4) by considering the Joule heating under adiabatic conditions:

$$T(t) = T_{\text{ini}} + \frac{R^2}{8} \int_0^t \frac{1}{\rho[B(\tau)]C_p[T(\tau)]} \left[\frac{dB(\tau)}{d\tau} \right] d\tau,$$

where R is the effective sample radius and C_p is the temperature-dependent specific heat of SmB_6 [41] (see Supplemental Material [10] for the detailed evaluation of the Joule heating effect). Other temperature-induced boundary points were evaluated from $\rho(T)$ using the PPMS and ND pulsed magnet (see also Supplemental Material [10] for the estimation of T^*). For a comparison with the transition field in the previous high-field studies using samples grown by the Al-flux method [11–13]; see Supplemental Material [10]. By connecting the boundary points, four independent states (S1, S2, M', and M) are defined in the T - B phase diagram. A finite magnetocaloric effect, which is ignored in the calculation of sample temperature during the magnetic field pulse, may cause a slight modification of the phase diagram.

Semiconducting state S1 is phenomenologically characterized by frequency-independent magnetoresistance and metallization at B_{hyb} . We know that B_{hyb} can be described as $k_B T_K / 2\mu_{\text{eff}}$ (T_K : Kondo temperature), because the hybridization gap Δ should be comparable to $k_B T_K$. Using $\mu_{\text{eff}} = 0.665 \mu_B$ (expected in the Γ_8 state [32]) and the empirical relationship $T_K \sim 3T_{\chi_{\text{max}}} = 180$ K [23], B_{hyb} becomes $k_B T_K / 2\mu_{\text{eff}} = 192$ T, which is roughly in good agreement with the experimental value of 180 T obtained in this work.

Since the Kondo hybridization is expected to collapse at fields beyond B_{hyb} , delocalization of f electrons possibly leads to magnetization saturation, and the high-field M phase is

likely to be a normal paramagnetic metal. A considerably small change in $\Delta(T)$ at temperatures well below T_K ($\sim 0.3\%$ at $T/T_K = 0.22$, evaluated from the guideline in Fig. 4) was also observed in another Kondo semiconductor (YbB_{12} [42]), suggesting that a weakly temperature-dependent $\Delta(T)$ could be a common feature in Kondo semiconductors.

The low-temperature semiconducting state S2 exhibits frequency-dependent magnetoresistance, and becomes metallic in the low-frequency transport at B_1 although the hybridization gap is still open. If spin-singlet in-gap quasiparticles such as the spin polaron are dominantly excited in the state S2, the magnetization should increase at the transition field B_1 . Such a “metamagnetic transition” has been observed in several valence-fluctuating Kondo metals [43–45]. Therefore, to unveil the detailed properties of quasiparticles in the S2 phase, it is necessary to investigate whether a metamagnetic jump takes place at B_1 .

Finally, the results obtained for SmB_6 are briefly compared with those for another correlated semiconductor, FeSi , which has an S-M transition field of 270 T [46]. As in SmB_6 , the in-gap states of FeSi dominate electron conduction at low temperatures. However, there are notable discrepancies between the magnetoresistance of SmB_6 and FeSi . The $\rho(B)$ values at ~ 700 MHz and ~ 50 kHz are practically the same in FeSi , and the magnetic-field region dominating the in-gap state continuously shrinks toward 80 K [46], in contrast to the dome-like state S2 shown in Fig. 4. These facts imply that the quasiparticle in the in-gap state of FeSi is qualitatively different from that of SmB_6 . The most striking difference between the two materials is the nature of the electrons involving the orbital hybridization: $\text{Sm}(5d)$ - $\text{Sm}(4f)$ electrons for SmB_6 and $\text{Fe}(3d)$ - $\text{Si}(3p)$ electrons for FeSi . The localization nature is significant in $4f$ electrons, resulting in more significant correlation and intermediate valence-related properties.

In summary, we have investigated the high-frequency magnetoresistance of SmB_6 under ultrahigh magnetic fields up to 320 T generated by an electromagnetic flux-compression generator and a temperature–magnetic field phase diagram was established. Significant frequency dependence of the excitation was observed in the low-temperature semiconducting state lower than $T^* = 12.5$ K, indicating in-gap quasiparticles such as a spin-polaronic state became dominant. A transition field ($B_1 \sim 80$ T) of the low-temperature semiconducting state occurs due to the suppression of in-gap quasiparticles without closing the hybridization gap. On the other hand, another temperature-independent semiconductor-metal transition was observed around 180 T, where the hybridization gap closes. This transition field intensity is substantially larger than those reported in previous studies, which should be qualitatively distinct from each other. The field-induced metallic phase above 180 T is probably a paramagnetic normal-metal phase where the Kondo hybridization is suppressed and the localized nature of the $4f$ electrons is restored.

ACKNOWLEDGMENTS

D.N. acknowledges partial financial support from Japan Society for the Promotion of Science KAKENHI (Grant No. JP19K03710). This work was also partly supported by Japan Society for the Promotion of Science KAKENHI Challenging Research (Pioneering) Grant No. JP20K20521. The authors are grateful to Professor S. Takeyama for constructing the EMFC magnet system; Mr. H. Sawabe for his diligent technical support; Professor K. Kindo for providing us with a nondestructive 60-T class pulsed magnet; Dr. W. Matsuhara, Mr. H. Nakayama, and Mr. T. Yamada for their help in preparing the SmB_6 crystal; and Dr. T. T. Terashima for providing a trigger for this research.

-
- [1] G. Aeppli and Z. Fisk, in *Comments on Modern Physics: Comments on Condensed Matter Physics*, Part B (Gordon & Breach, 1992), Vol. 16, p. 155.
- [2] Z. Fisk, J. L. Sarrao, S. L. Cooper, P. Nyhus, G. S. Boebinger, A. Passner, and P. C. Canfield, *Phys. B: Condens. Matter* **206–207**, 798 (1995).
- [3] A. Menth, E. Buehler, and T. H. Geballe, *Phys. Rev. Lett.* **22**, 295 (1969).
- [4] B. Gorshunov, N. Sluchanko, A. Volkov, M. Dressel, G. Knebel, A. Loidl, and S. Kunii, *Phys. Rev. B* **59**, 1808 (1999).
- [5] X. Zhang, N. P. Butch, P. Syers, S. Ziemak, R. L. Greene, and J. Paglione, *Phys. Rev. X* **3**, 011011 (2013).
- [6] P. Hlawenka, K. Siemensmeyer, E. Weschke, A. Varykhalov, J. Sánchez-Barriga, N. Y. Shitsevalova, A. V. Dukhnenko, V. B. Filipov, S. Gabáni, K. Flachbart, O. Rader, and E. D. L. Rienks, *Nat. Commun.* **9**, 517 (2018).
- [7] H. Pirie, Y. Liu, A. Soumyanarayanan, P. Chen, Y. He, M. M. Yee, P. F. S. Rosa, J. D. Thompson, D. J. Kim, Z. Fisk, X. Wang, J. Paglione, D. K. Morr, M. H. Hamidian, and J. E. Hoffman, *Nat. Phys.* **16**, 52 (2020).
- [8] L. Li, K. Sun, C. Kurdak, and J. W. Allen, *Nat. Rev. Phys.* **2**, 463 (2020).
- [9] L. Jiao, S. Röbber, D. J. Kim, L. H. Tjeng, Z. Fisk, F. Steglich, and S. Wirth, *Nat. Commun.* **7**, 13762 (2016).
- [10] See Supplemental Material at <http://link.aps.org/supplemental/10.1103/PhysRevB.105.L241105> for experimental setup, magnetic properties, low-temperature magnetoresistance, additional high-field data, Joule heating effect, comparison with other high-field studies, schematic band structure, and comment on the pressure-induced transition, which includes Refs. [8,11–19].
- [11] F. Chen, C. Shang, Z. Jin, D. Zhao, Y. P. Wu, Z. J. Xiang, Z. C. Xia, A. F. Wang, X. G. Luo, T. Wu, and X. H. Chen, *Phys. Rev. B* **91**, 205133 (2015).
- [12] M. Shahrokhvand, S. Pezzini, M. R. van Delft, U. Zeitler, N. E. Hussey, and S. Wiedmann, *Phys. Rev. B* **96**, 205125 (2017).
- [13] J. C. Cooley, C. H. Mielke, W. L. Hulst, J. D. Goettee, M. M. Honold, R. M. Modler, A. Lacerda, D. G. Rickel, and J. L. Smith, *J. Supercond.* **12**, 171 (1999).
- [14] J. Derr, G. Knebel, D. Braithwaite, B. Salce, J. Flouquet, K. Flachbart, S. Gabáni, and N. Shitsevalova, *Phys. Rev. B* **77**, 193107 (2008).
- [15] D. Nakamura, A. Ikeda, H. Sawabe, Y. H. Matsuda, and S. Takeyama, *Rev. Sci. Instrum.* **89**, 95106 (2018).

- [16] D. Nakamura, M. M. Altarawneh, and S. Takeyama, *Meas. Sci. Technol.* **29**, 035901 (2018).
- [17] K. Akintola, A. Pal, S. R. Dunsiger, A. C. Y. Fang, M. Potma, S. R. Saha, X. Wang, J. Paglione, and J. E. Sonier, *npj Quantum Mater.* **3**, 36 (2018).
- [18] N. E. Sluchanko, V. V. Glushkov, B. P. Gorshunov, S. V. Demishev, M. V. Kondrin, A. A. Pronin, A. A. Volkov, A. K. Savchenko, G. Grüner, Y. Bruynseraede, V. V. Moshchalkov, and S. Kunii, *Phys. Rev. B* **61**, 9906 (2000).
- [19] N. Miura, Y. H. Matsuda, K. Uchida, S. Todo, T. Goto, H. Mitamura, T. Osada, and E. Ohmichi, *Phys. B: Condens. Matter* **294–295**, 562 (2001).
- [20] M. Mizumaki, S. Tsutsui, and F. Iga, *J. Phys.: Conf. Ser.* **176**, 012034 (2009).
- [21] Y. Utsumi, D. Kasinathan, K. T. Ko, S. Agrestini, M. W. Haverkort, S. Wirth, Y. H. Wu, K. D. Tsuei, D. J. Kim, Z. Fisk, A. Tanaka, P. Thalmeier, and L. H. Tjeng, *Phys. Rev. B* **96**, 155130 (2017).
- [22] C. E. Matt, H. Pirie, A. Soumyanarayanan, Y. He, M. M. Yee, P. Chen, Y. Liu, D. T. Larson, W. S. Paz, J. J. Palacios, M. H. Hamidian, and J. E. Hoffman, *Phys. Rev. B* **101**, 085142 (2020).
- [23] F. Iga, N. Shimizu, and T. Takabatake, *J. Magn. Magn. Mater.* **177–181**, 337 (1998).
- [24] M. C. Hatnean, M. R. Lees, D. M. K. Paul, and G. Balakrishnan, *Sci. Rep.* **3**, 3071 (2013).
- [25] S. Wolgast, Y. S. Eo, K. Sun, C. Kurdak, F. F. Balakirev, M. Jaime, D. J. Kim, and Z. Fisk, *Phys. Rev. B* **95**, 245112 (2017).
- [26] P. Syers, D. Kim, M. S. Fuhrer, and J. Paglione, *Phys. Rev. Lett.* **114**, 096601 (2015).
- [27] S. Biswas, R. Nagarajan, S. Sarkar, K. R. Amin, M. Ciomaga Hatnean, S. Tewari, G. Balakrishnan, and A. Bid, *Phys. Rev. B* **92**, 085103 (2015).
- [28] E. S. Konovalova, Y. B. Paderno, T. Lundstrom, L. D. Finkel'shtein, N. N. Efremova, and E. M. Dudnik, *Sov. Powder Metall. Met. Ceram.* **21**, 820 (1982).
- [29] W. A. Phelan, S. M. Koohpayeh, P. Cottingham, J. A. Tutmaher, J. C. Leiner, M. D. Lumsden, C. M. Lavelle, X. P. Wang, C. Hoffmann, M. A. Siegler, N. Haldolaarachchige, D. P. Young, and T. M. McQueen, *Sci. Rep.* **6**, 20860 (2016).
- [30] W. A. Phelan, S. M. Koohpayeh, P. Cottingham, J. W. Freeland, J. C. Leiner, C. L. Broholm, and T. M. McQueen, *Phys. Rev. X* **4**, 031012 (2014).
- [31] T. T. Terashima, A. Ikeda, Y. H. Matsuda, A. Kondo, K. Kindo, and F. Iga, *J. Phys. Soc. Jpn.* **86**, 054710 (2017).
- [32] R. Higashinaka, A. Yamada, T. D. Matsuda, and Y. Aoki, *AIP Adv.* **8**, 125017 (2018).
- [33] P. A. Alekseev, V. N. Lazukov, R. Osborn, B. D. Rainford, I. P. Sadikov, E. S. Konovalova, and Y. B. Paderno, *Europhys. Lett.* **23**, 347 (1993).
- [34] S. Curnoe and K. A. Kikoin, *Phys. Rev. B* **61**, 15714 (2000).
- [35] N. E. Sluchanko, A. A. Volkov, V. V. Glushkov, B. P. Gorshunov, S. V. Demishev, M. V. Kondrin, A. A. Pronin, N. A. Samarin, Y. Bruynseraede, V. V. Moshchalkov, and S. Kunii, *J. Exp. Theor. Phys.* **88**, 533 (1999).
- [36] N. E. Sluchanko, V. V. Glushkov, S. V. Demishev, A. A. Pronin, A. A. Volkov, M. V. Kondrin, A. K. Savchenko, and S. Kunii, *Phys. Rev. B* **64**, 153103 (2001).
- [37] S. V. Demishev, A. N. Azarevich, A. V. Bogach, M. I. Gilmanov, V. B. Filipov, N. Y. Shitsevalova, and V. V. Glushkov, *JETP Lett.* **109**, 150 (2019).
- [38] S. V. Demishev, M. I. Gilmanov, A. N. Samarin, A. V. Semeno, N. E. Sluchanko, N. A. Samarin, A. V. Bogach, N. Y. Shitsevalova, V. B. Filipov, M. S. Karasev, and V. V. Glushkov, *Appl. Magn. Reson.* **51**, 71 (2020).
- [39] K. Flachbart, M. Bartkowiak, S. Demishev, S. Gabani, V. Glushkov, T. Herrmannsdorfer, V. Moshchalkov, N. Shitsevalova, and N. Sluchanko, *Phys. B: Condens. Matter* **404**, 2985 (2009).
- [40] T. Kasuya, K. Takegahara, T. Fujita, T. Tanaka, and E. Bannai, *J. Phys. Colloq.* **40**, C5-308 (1979).
- [41] M. Orendáč, S. Gabáni, G. Pristáš, E. Gažo, P. Diko, P. Farkašovský, A. Levchenko, N. Shitsevalova, and K. Flachbart, *Phys. Rev. B* **96**, 115101 (2017).
- [42] Y. H. Matsuda, Y. Kakita, and F. Iga, *Crystals* **10**, 26 (2020).
- [43] P. Haen, J. Flouquet, F. Lapiere, P. Lejay, and G. Remenyi, *J. Low Temp. Phys.* **67**, 391 (1987).
- [44] R. Settai, A. Misawa, S. Araki, M. Kosaki, K. Sugiyama, T. Takeuchi, K. Kindo, Y. Haga, E. Yamamoto, and Y. Onuki, *J. Phys. Soc. Jpn.* **66**, 2260 (1997).
- [45] Y. H. Matsuda, T. Nakamura, J. L. Her, K. Kindo, S. Michimura, T. Inami, M. Mizumaki, N. Kawamura, M. Suzuki, B. Chen, H. Ohta, and K. Yoshimura, *J. Phys. Soc. Jpn.* **81**, 015002 (2012).
- [46] D. Nakamura, Y. H. Matsuda, A. Ikeda, A. Miyake, M. Tokunaga, S. Takeyama, and T. Kanomata, *Phys. Rev. Lett.* **127**, 156601 (2021).